# A Light-Responsive Release Platform by Controlling the Wetting Behavior of Hydrophobic Surface

**Linfeng Chen,[†,‡] Wenqian Wang,[§] Bin Su,[†] Yongqiang Wen,[§,*] Chuanbao Li,[§] Yabin Zhou,[§] Mingzhu Li,[†] Xiaodi Shi,[†,‡] Hongwu Du,[§] Yanlin Song,[†,*] and Lei Jiang[†]**

[†]Key laboratory of Green Printing, Key Lab of Organic Solids, Beijing National Laboratory for Molecular Sciences (BNLMS), Institute of Chemistry, Chinese Academy of Sciences, Beijing 100190, P. R. China, [‡]University of Chinese Academy of Sciences, Beijing 100049, P.R. China, and [§]Research Center for Bioengineering & Sensing Technology, University of Science and Technology Beijing, Beijing 100083, China

**ABSTRACT** Controlled release system based on mesoporous silica (MS) nanomaterials has drawn great attention over the past decades due to its potential biomedical applications. Herein, a light-responsive release system based on MS nanoparticles was achieved by adjusting the wetting of the MS surface. At the starting stage, the surface of MS modified with optimal ratio of spiropyran to fluorinated silane (MS-FSP) was protected from being wetted by water, successfully inhibiting the release of model cargo molecules, fluorescein disodium (FD). Upon irradiation with 365 nm UV light, the conformational conversion of spiropyran from a "closed" state to an "open" state caused the surface to be wetted, leading to the release of FD from the pores. The further *in vitro* studies demonstrated the system loaded with anticancer drug camptothecin (CPT) could be effectively controlled to release the drug by UV light stimuli to enhance cytotoxicity for EA.hy926 cells and HeLa cells. This wettability-determined smart release platform could be triggered by remote stimuli, which might hold promise in the applications of drug delivery and cancer therapy.

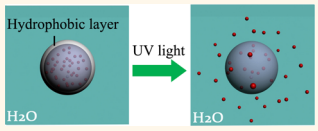


**KEYWORDS:** mesoporous silica · spiropyran · light-responsive · controlled release · wetting

Hydrophobicity is a common phenomenon in Nature.[1−3] Investigation and utilization of the hydrophobic property has received considerable attention for many years because of its various applications in water collection,[4,5] self-cleaning,[6,7] liquid transportation,[8−10] and oil−water separation.[11,12] In the natural word, an ion channel in biological membranes, *e.g.*, $K^+$ ion channel, was found to control the permeation of ions and molecules across the membranes by alternating the cavity hydrophobicity,[13,14] which encouraged the researchers to fabricate artificial nanopores to mimic the function of ion channels.[15,16] Inspired by Nature, we expect the hydrophobic effect could be utilized as an effective strategy to control the release of guest molecules from the container.

Controlled release plays an important role in therapeutics, imaging, and diagnosis.[17,18] Over the past decade, particular attention has been paid to the mesoporous silica (MS) nanoparticles-based controlled release systems, which provide a potential and multifunctional platform for biomedical application.[19−25] To achieve the delivery and release of cargo molecules, the access to pore opening was generally controlled by nanopistons on the surface of MS, such as Au nanoparticles,[22,23] CdS nanoparticles,[19] $Fe_3O_4$ nanoparticles,[26] and supramolecules.[27−29] Polymers were also used to control the opening/closing of passageways,[30,31] realizing the controlled release process by stimulus.[32−34] Despite the increasing growth of reports, to develop a simple and high-performance controlled release system is still highly desired. Recently, Grinstaff *et al.* reported a superhydrophobic polymer material for tunable drug release, in which hydrophobic effect was used as an alternative strategy to regulate the release of guest molecules.[35] However; the release process cannot be controlled, and the premature release cannot be avoided due to the lack of real-time responsiveness, which motivated us to explore a novel smart release system controlled by external stimuli.

Herein, a light-responsive release system was designed and fabricated by controlling the wetting behavior of the surface of MS.

* Address correspondence to ylsong@iccas.ac.cn, wyq_wen@ustb.edu.cn.

Received for review October 16, 2013 and accepted January 2, 2014.

**Published online January 02, 2014**
**10.1021/nn405398d**

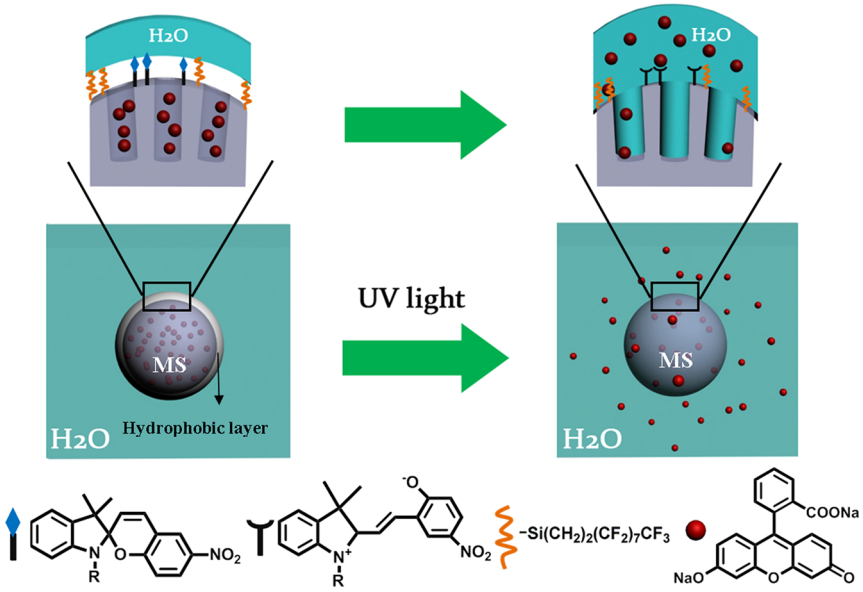


**Figure 1. The schematic of the light-responsive release system. The outer surface of MS was functionalized with spiropyran and perfluorodecyltriethoxysilane in an optimal ratio (0.249:1) which could prevent the surface from being wetted by water, and block the loaded cargos. After irradiation with 365 nm UV light, the surface became wetted due to the conformational conversion of spiropyran from the "closed" form to the "open" form, and the encapsulated fluorescein disodium molecules diffused from the pores.**

Spiropyran, a photosensitive molecule which was widely studied for its switchable properties,[36−38] was chosen as the gate molecule due to its different hydrophobicity between the "closed" and "open" forms.[39,40] Fluorinated silane was selected to mix with spiropyran to help achieve the overall hydrophobic state according to the reported method.[41] Such hydrophobic dopant could help to protect the surface from being wetted by water and inhibit the release of encapsulated molecules. Under UV irradiation at 365 nm, spiropyran was converted to the hydrophilic form, which resulted in the wetting of surface of MS and the release of trapped molecules diffusing from the penetrated water (Figure 1). This simple light-responsive release system, free of blockers, provides a new platform for highly efficient controlled release, which might hold promise in the applications of nanomedicine, nanopore device and other fields.

## RESULTS AND DISCUSSION

The employed MS was prepared by modified base-catalyzed sol−gel method.[22,42] As shown in Figure 2, spherical MS particles with an average diameter 300 nm were obtained (Figure 2a). The mesoporous channel could be clearly observed by transmission electron microscopy (Figure 2b). $N_2$ sorption analysis of MS exhibited a type *IV* isotherm with a total surface area (Brunauer−Emmett−Teller, BET) of 1291.1 $m^2\,g^{-1}$ and an average pore diameter of 2.7 nm (Figure 2c). The nanoparticles also showed typical XRD patterns of MCM-41-type hexagonal mesoporous silica with a lattice spacing of *ca.* 4.2 nm (Figure 2d).

Carboxylic acid-terminated spiropyran (SP-COOH) was first synthesized by one-step reaction (Figure S1).[39] Then, MS was treated with the mixture of 3-aminopropyltriethoxy-silane (APTES) and perfluorodecyltriethoxysilane (PFDTES) to afford amine- and fluorinated silane-modified MS (MS-$FNH_2$), which was then reacted with SP-COOH to form the final red product MS-FSP (Figure S2). The functionalized MS was characterized by Fourier transform infrared spectroscopy (FTIR, Figure 3). In the FTIR spectrum of MS-$FNH_2$, the absorption peak at 1484 $cm^{-1}$ was attributed to the vibrations of amino group, and the absorption peaks at 2966 and 2855 $cm^{-1}$ were produced by the vibration of $-CH_2-$ group, while the peak at 1213 $cm^{-1}$ was due to the C−F vibration. The results confirmed the successful immobilization of amino and fluoroalkyl group on the surface of MS. In the FTIR spectrum of MS-FSP, the absorption bands at 1647 and 1725 $cm^{-1}$ were assigned to the vibration of the amide and ester groups, respectively, indicating the successful attachment of spiropyran to MS. Also, the MS-FSP was characterized by solid-state $^{13}C$ NMR spectroscopy and XPS. The peaks at 178.3 and 173.7 ppm were produced by the spiropyran moiety (Figure S3), and the XPS spectra showed the existence of F (Figure S6), which further confirmed the successful modification of spiropyran and fluorinated silane to the surface of MS.

In this research, fluorescein disodium (FD) was chosen as the model cargo. The absorption and emission peaks of FD solution were centered at 487 and 511 nm, respectively, as illustrated in Figure S4. The loading of FD was achieved by dispersing the MS-FSP sample

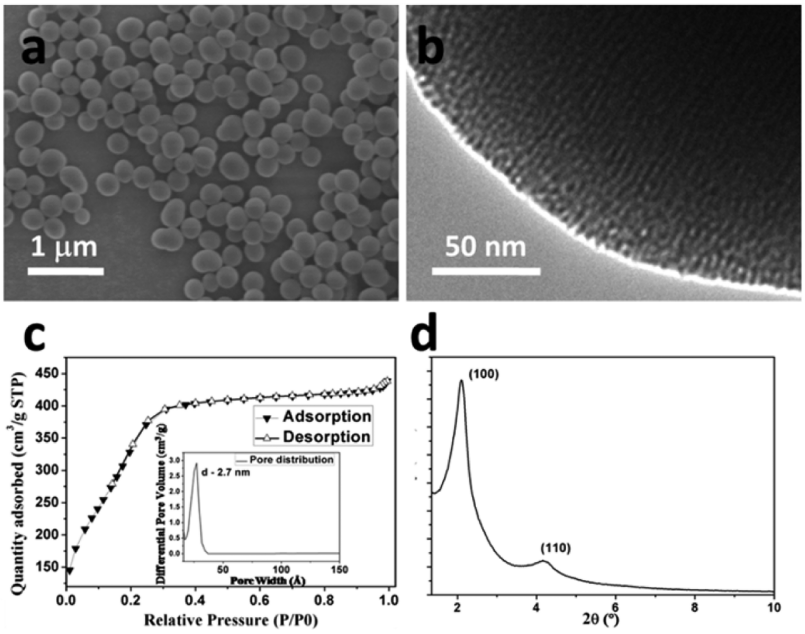


**Figure 2. The characterizations of mesoporous silica nanomaterials (MS). (a) SEM, the average of MS was 300 nm. (b) TEM, the mesoporous channel was clearly observed. (c) $N_2$ sorption isotherm (inset: pore size distribution), the total surface area (BET) was about 1291.1 $m^2$ $g^{-1}$ with average pore diameter of 2.7 nm. (d) XRD, the nanoparticles showed typical XRD patterns of MCM-41-type hexagonal mesoporous silica with a lattice spacing of *ca.* 4.2 nm.**

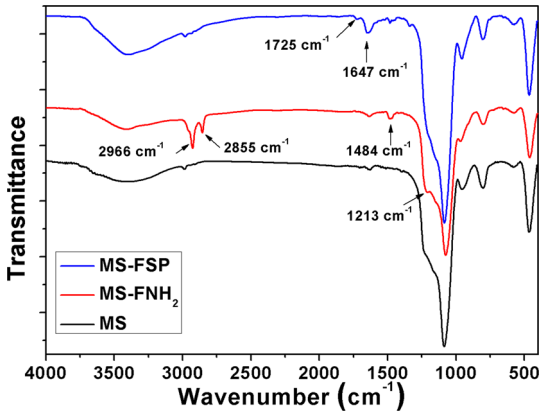


**Figure 3. The characterization of functionalization of MS by FTIR. Amine- and fluorinated silane-modified MS (MS-$FNH_2$) exhibited new absorption peaks at 2966, 2855, 1484, and 1213 $cm^{-1}$ (red curve). Final spiropyran-modified MS (MS-FSP) displayed typical absorption bands at 1725 and 1647 $cm^{-1}$ (blue curve).**

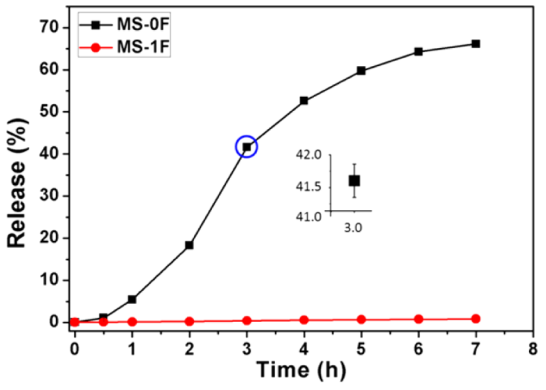


**Figure 4. The release profile of fluorescein disodium molecules from samples in PBS solution (0.1 M, pH 7.2) as a function of time. MS without modification (MS-0F, black curve) showed rapid release while MS grafted with fluorinated silane (MS-1F, red curve) exhibited negligible release in 7 h. The inset was the enlarged data demarked by the blue circle.**

(500 mg) by sonication into 10 mL of ethanol solution containing FD ($10^{-3}$ M) for *ca.* 8 h. The water/ethanol volume ratio was about 4/1. Then, the FD-loaded samples were collected by centrifugation, washed with water, and dried at 50 °C under vacuum for 24 h before the investigations of the release behavior. Time-resolved fluorescence spectrum was employed to monitor the release process by fluorescence detection at 511 nm.

To obtain the evidence that the hydrophobic effect could inhibit the release of guest molecules from the pores of MS, MS samples grafted with only PFDTES molecules (MS-1F) were prepared to acquire a hydrophobic surface. About 5 mg of MS-1F was placed in the bottom of cuvette, and kept submerged in 1 mL of PBS solution (0.1 M, pH 7.2). The release behavior was recorded by plotting the intensity of fluorescence signal *versus* time. As exhibited in Figure 4, MS-1F showed negligible release within 7 h (red curve). However, in a control experiment, MS sample without any modification (MS-0F), which has a hydrophilic surface, showed a rapid release behavior during the same time period (black curve). The results indicated that the hydrophobic effect can efficiently prevent the surface of samples from being wetted by water and could be utilized as an efficient strategy to trap cargos.

The light-responsive release behavior of MS-FSP was then investigated. The photoisomerization of spiropyran attached on the surface of MS could be confirmed by UV−vis spectra under alternative UV and visible light irradiation (Figure S5). To achieve the light-triggered release, the surface of MS should be functionalized with an appropriate ratio of spiropyran to PFDTES. The actual molar ratio was determined by X-ray photoelectron spectroscopy (XPS, Figure S6 and Table S1). As exhibited in Figure S7, in the case of sample grafted with only spiropyran (MS-SP), it showed rapid release, which indicated FD molecules would escape from the pores without hydrophobic effect (black curve). Moreover, when the ratio of spiropyran to PFDTES was high (2.57:1; 0.949:1), the hydrophobicity of the samples could not repel the water and FD quickly released with little difference before and after UV irradiation, which confirmed the FD was mainly inside the pores but not on the surface by adsorption (MS-FSP-1, red curve and MS-FSP-2, blue curve). However, when the ratio of spiropyran to PFDTES was low (0.172:1; 0.03:1), the surface was so highly hydrophobic that FD could hardly run out of the pores (MS-FSP-4, green curve and MS-FSP-5, pink curve). In this research, the optimal molar ratio that favored the photoresponsive release of FD molecules was found to be around 0.249:1 (MS-FSP-3 in Figure S6 and Table S1; in the following text, MS-FSP-3 was defined as MS-FSP). The loading content of MS-FSP was about 0.699 $\mu$g/mg determined by fluorescence spectroscopy. It exhibited negligible release without UV light irradiation (black curve) within 12 h and displayed obvious release upon exposure to UV light irradiation, as presented in Figure 5. After the initial 24 h, the release became slower (Figure S8). The results indicated that the release could be triggered by light which was a clean and site specific method.

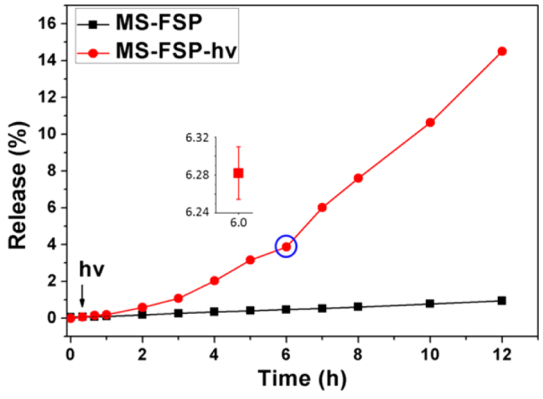


**Figure 5. The release profile of fluorescein disodium molecules from MS-FSP samples in PBS solution (0.1 M, pH 7.2) *versus* time. The sample modified with optimal molar ratio of spiropyran to PFDTES (0.249:1) displayed poor release in 12 h without 365 UV light irradiation (black curve). However, after 365 UV light irradiation for 5 min, the sample remained sustainable release (red curve). The inset was the enlarged data demarked by blue circle.**

The wetting behavior of the surface was proposed to be responsible for the release process. At the starting stage, the surface of MS-FSP coated with spiropyran and fluorinated silane in optimal ratio was hydrophobic, which protected the surface from being wetted in aqueous solution. As a consequence, the encapsulated FD could not release from the pores. However, under UV light irradiation, the surface of MS-FSP was wetted as a result of the conformational conversion of spiropyran from the hydrophobic, closed form to the hydrophilic, open form, leading to the release of guest molecules. The wetting process of surface could be assessed by water adhesion change detected on silicon slide with 5 $\mu$m square micropillar structures, which was decorated with the same component as MS-FSP. Before UV light irradiation, the surface with hydrophobicity was dewetted by water, and the low adhesion (39.0 $\pm$ 2.7 $\mu$N) was displayed (Figure 6A). After exposure to 365 nm UV light for 5 min, however, the spiropyran was switched from the hydrophobic form to the hydrophilic form, which led to the wetting of the surface by water and the increase of adhesion up to 88.7 $\pm$ 13.1 $\mu$N. A water droplet was finally snapped off from the cap (Figure 6B). The results indicated the release was due to the wetting process of surface induced by light irradiation. Compared with the results reported by J. Locklin *et al.*,[43] the surface was more hydrophobic (128.2 $\pm$ 3.0°), which was important to protect the surface from being wetted by water, and did not present contact angle change after UV light irradiation but only the wetting of surface was observed.

This system might hold promise for drug delivery and release, imaging, and diagnosis. Herein, we incubated the samples with EA.hy926 and HeLa cells to demonstrate the feasibility of *in vitro* controlled release. Anticancer drug camptothecin (CPT) was chosen as the active agent and loaded into MS-FSP (MS-FSP-CPT). The loading content was about 9.97 $\mu$g/mg characterized by fluorescence spectroscopy (Figure S9). The UV light-responsive release performance of MS-FSP-CPT in solution was similar to that loaded with FD (Figure S10). In the *in vitro* experiment, EA.hy926 and HeLa cells were first independently cultured in

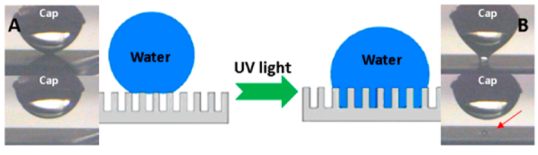


**Figure 6. The mechanism illustrating the wetting process of surface. The silicon with micropillar structure was modified with the same molar ratio of spiropyran to PFDTES (0.249:1) as MS-FSP sample. Before UV light irradiation, the surface was hydrophobic, exhibiting low water adhesion (39.0 $\pm$ 2.7 $\mu$N) (A). After exposure to 365 nm UV light, the surface became wetted by water, and displayed high water adhesion (88.7 $\pm$ 13.1 $\mu$N), leaving a water droplet on the surface (B).**

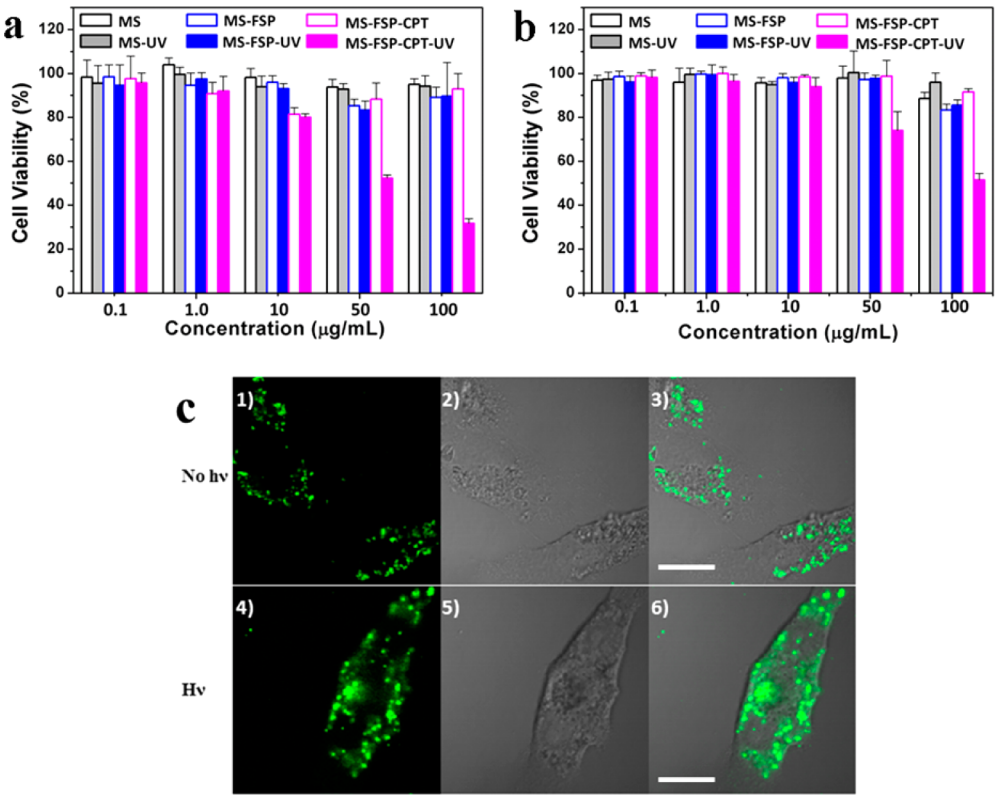


**Figure 7. (a) EA.hy926 and (b) HeLa cell viability measured by 3-[4,5-dimethylthiazol-2-yl]-2,5-diphenyltetrazolium bromide (MTT) assay after separate incubation with MS, MS-FSP and MS-FSP-CPT samples (0.1, 1.0, 10, 50, and 100 $\mu$g/mL) for 24 h. Blank bar represented samples without UV light irradiation while solid bar represented samples with UV light irradiation (2.4 $\mu$W/cm$^2$) for 5 min. (c) Confocal fluorescence and bright images corresponding to EA.hy926 cells incubated with FD-loaded MS-FSP (50 $\mu$g/mL) without (1, 2, 3) and with (4, 5, 6) UV light irradiation for 5 min. (1 and 4) Fluorescence ($\lambda_{ex}$ = 488 nm); (2 and 5) bright field; (3 and 6) the overlay image of (1) (2) and (4) (5). The scale-bar corresponds to 20 $\mu$m.**

96-well plates for 12 h. Subsequently, MS, MS-FSP, and MS-FSP-CPT with different concentration (0.1, 1.0, 10, 50, and 100 $\mu$g/mL) were separately incubated with the cells. After 24 h incubation, the cell viability was determined. As a control experiment, the other group set of cells was exposed to UV light irradiation (2.4 $\mu$W/cm$^2$) for 5 min after being separately incubated with MS, MS-FSP, and MS-FSP-CPT for 2 h, and the cell viability was detected after 24 h. As illustrated in Figure 7, both MS and MS-FSP exhibited little cytotoxicity even when the concentration increased up to 100 $\mu$g/mL. Upon UV light irradiation, no loss of cell viability was observed. The results demonstrated the system was biocompatible. However, in the case of MS-FSP-CPT-incubated cells, an obvious loss of cell viability was observed when the MS-FSP-CPT concentration reached 50 $\mu$g/mL upon UV light exposure compared to that without UV light irradiation, which was attributed to the light-triggered release of CPT within cells. When the concentration of MS-FSP-CPT increased up to 100 $\mu$g/mL, cell viability was decreased down to nearly 32% (EA.hy926) and 51% (HeLa cells) upon UV light exposure. As free CPT did not exhibit obvious cytotoxicity to cells until the concentration reached up to 0.625 $\mu$g/mL (EA.hy926) and 1.25 $\mu$g/mL (HeLa cells), as shown in Figure S11a,b, the higher toxicity of MS-FSP-CPT system upon UV irradiation was ascribed to the efficient CPT release within cells triggered by UV light. In addition, the effective endocytosis of MS-FSP by EA.hy 926 cells and HeLa cells was confirmed by confocal microscopy. After 12 h incubation of FD-loaded MS-FSP with EA.hy 926 cells and HeLa cells, the cells were washed by PBS solution and viewed by confocal microscopy (Figure 7c and Figure S11c). Without UV light irradiation, there was no obviously release of FD in the cells (Figure 7c 1, 2, 3, and Figure S11c 1, 2, 3). After UV stimuli was applied, FD (green) was found spread in the cell cytoplasm in cells, which demonstrated the successful release of FD molecules (Figure 7c 4, 5, 6, and Figure S11c 4, 5, 6).

## CONCLUSION

In summary, a light-responsive release system was achieved through the control of the wetting behavior of MS surface. FD and CPT molecules could be trapped in the mesopores due to the hydrophobic effect. Under UV light irradiation, the wetting of the surface resulted in the release of the cargos due to the conformational change of spiropyran. The smart carrier was also demonstrated to efficiently delivery and release CPT drug

*in vitro* triggered by UV light stimuli to enhance cytotoxicity for EA.hy926 and HeLa cells. This release platform is free of block units and could be manipulated by light. The general strategy opens up new possibilities for constructing drug delivery and controlled release systems from the point of view of surface.

## EXPERIMENTAL SECTION

**Materials.** Tetraethoxysilane (TEOS, 28%), *n*-cetyltrimethylammonium bromide (CTAB, ≥99%), 3-aminopropyltriethoxysilane (APTES, 99%), perfluorodecyltriethoxysilane (PFDTES, 97%), succine anhydride (99%), *N*-hydroxy-succinimide (NHS, 98%), 4-dimethylaminopyridine (DMAP, ≥99%), fluorescein disodium (FD), 1-ethyl-3-(3-dimethylaminopropyl)carbodiimide-HCl (EDC, 99%), and 3-[4,5-dimethylthiazol-2-yl]-2,5-diphenyltetrazolium bromide (MTT, ≥98%) were purchased from Sigma-Aldrich Company. 3′,3′-Dimethyl-6-nitrol-spiro[2*H*-1-benzopyran-2,2′-indoline]-1′-ethanol (spiropyran, SP−OH, >93.0%), and camptothecin (CPT, >98%) were purchased from J&K Scientific. Dulbecco's Modified Eagle Medium (DMEM) and fetal bovine serum (FBS) were purchased from HyClone. All phosphate-buffered saline (PBS, 0.1 M, pH 7.2) was prepared with ultrapure Milli-Q water (resistance >18 MΩ $cm^{-1}$). All chemicals were used without further purification.

**Instruments and Characterization.** Scanning electron microscope (SEM) images were obtained with a JEOL-7500FE instrument. Transmission electron microscopy (TEM) was performed using a Philips CM operated at 200 kV. Powder XRD diffraction patterns were collected on a Rigaku D/max 2500 using Cu Kα radiation. Fluorescence spectra were taken on a Hitachi F-4500 FL Spectrophotometer. Fourier transform infrared spectra (FTIR) were recorded on a Bruker-EQUINOX55 spectrometer. All spectra were recorded with an instrument resolution of 4 $cm^{-1}$. UV−visible spectra were taken on UV-4100 spectrometer. $N_2$ absorption and desorption isotherms were measured at 77 K on a Micromeritics ASAP2020 automated sorption analyzer. The Brunauer−Emmett−Teller (BET) model was used to calculate the specific surface areas. Pore size and distribution were calculated from the absorption data by following the Barrett−Joyner−Halenda (BJH) method. X-ray photoelectron spectra (XPS) were carried out on ESCALab220i-XL. The adhesion force was assessed by microelectromechanical balance system (Kruss) equipped with a home-built platinum semispherical cap to hold Milli-Q water (10 μL). $^1H$ and $^{13}C$ NMR spectra were measured in $CDCl_3$/pyr-$d_5$/MeOD (with TMS as internal standard) on a Bruker AV300 ($^1H$ at 300 MHz, $^{13}C$ at 75 MHz) magnetic resonance spectrometer. The solid-state $^{13}C$ NMR spectroscopy was recorded on AVANCE III 400 (400 M) by using a powered sample. Chemical shifts ($\delta$) are reported in ppm, and coupling constants ($J$) are in Hz. The confocal microscopy images of cancer cells were performed with Olympus FV1000-IX81.

**Preparation of MS.** The mesoporous silica nanoparticles (MS) were prepared with the modified method as described previous.[22]

**Preparation of SP−COOH.** SP−OH (1.6 g) was added into dichloromethane solution (120 mL) containing succine anhydride (570 mg), 4-dimethylaminopyridine (DMAP, 200 mg), and triethylamine (3 mL), and the mixture was stirred for 24 h at room temperature, followed by the solvent removal under vacuum. The crude product was purified by silica gel flash chromatography eluting with a 50% acetic ester to petroleum ether eluent to give finally yellow powder production SP−COOH (1.62 g, 81%). $^1H$ NMR (300 MHz, $CDCl_3$) $\delta$ 8.00 (d, $J$ = 6.7 Hz, 2H), 7.20 (t, $J$ = 7.6 Hz, 1H), 7.09 (d, $J$ = 7.2 Hz, 1H), 6.95−6.83 (m, 2H), 6.70 (dd, $J$ = 22.8, 8.7 Hz, 2H), 5.88 (d, $J$ = 10.4 Hz, 1H), 4.37−4.14 (m, 2H), 3.57−3.33 (m, 2H), 2.60 (dd, $J$ = 17.3, 5.6 Hz, 4H), 1.28 (s, 3H), 1.16 (s, 3H). $^{13}C$ NMR (75 MHz, $CDCl_3$) $\delta$ 177.98, 171.98, 159.40, 146.62, 141.09, 135.72, 128.39, 127.87, 125.97, 122.82, 121.88, 121.72, 119.97, 118.45, 115.55, 106.66, 106.47, 62.83, 52.84, 42.38, 28.73, 28.65, 25.87, 19.86.

**Preparation of MS-FSP.** The as-prepared MS (0.3 g) was first added with the mixture of APTES and PFDTES with different molar ratio in dry toluene (15 mL) to give amine- and fluorinated silane-modified MS (denoted as MS-$FNH_2$-*X* (X = 1∼5)). In details, MS-$NH_2$-*X* was obtained by adding with the following volume of APTES and PFDTES: (0.281 mL, 0.131 mL), (0.218 mL, 0.135 mL), (0.158 mL, 0.293 mL), (0.117 mL, 0.4335 mL), and (0.071 mL, 0.519 mL). The reaction was carried out for 1 h under stirring. Then, the samples were recovered by centrifugation, and placed into oven at 120 °C for 3 h to obtain (MS-$FNH_2$-*X*, *X* = 1∼5). After the surfactant template was removed by acetone extraction for 48 h, MS-$FNH_2$-X (*X* = 1∼5) were dispersed by sonication into ethanol solution containing SP-COOH (355, 276, 197, 148, and 90 mg), EDC (2 mL), and NHS (1 mL), and reacted at room temperature for 24 h, and the solution was then centrifuged and washed with water several times. The final samples (MS-FSP-*X*, *X* = 1∼5) were dried at 50 °C under vacuum for 24 h.

**Loading of Guest Molecules.** To load FD, MS-FSP (500 mg) was dispersed by sonication into 10 mL of ethanol solution containing FD ($10^{-3}$ M) for 8 h. The water/ethanol volume ratio was about 4/1. Then, samples were recovered by centrifugation, washed with water several times, and finally dried at 50 °C under vacuum for 24 h to give FD-loaded samples. To load anticancer drug CPT, MS-FSP (100 mg) was dispersed by sonication in DMSO containing CPT ($10^{-3}$ M) for 8 h. Then, CPT-loaded MS-FSP was collected by centrifugation, washed with water several times, and finally dried at 50 °C under vacuum for 24 h.

**Loading Efficiency Evaluation.** The FD and CPT loading contents of MS-FSP were determined by fluorescence spectroscopy. The standard curves of FD and CPT were established. The fluorescence intensity of FD was recorded by monitoring the signal at 511 nm (excitation at 487 nm) while that of CPT was detected by monitoring the signal at 447 nm (excitation at 380 nm), respectively.

**Release Measurement.** About 5 mg of sample was placed in the bottom of cuvette, and kept submerged in 1 mL of PBS solution (0.1 M, pH 7.2) at 37 °C during the release process. The release of FD molecules was monitored by detection the wavelength at 511 nm using 487 nm light to excite the molecules. The release of CPT cargos was detected by monitoring the signals at 447 nm with 380 nm as the exciting light.

**Cell Experiment.** EA.hy926 and HeLa cells were placed on 96 well cell culture clusters at a density of $2 \times 10^4$ cells per well and cultured in 5% $CO_2$ at 37 °C for 12 h. Subsequently, assisted with ultrasonication, MS, MS-FSP and camptothecin-loaded MS-FSP with different concentrations (0.1, 1.0, 10, 50, and 100 μg/mL), which were dispersed in aqueous solution containing sodium docecylbenzenesulfonate surfactant (SDBS, $10^{-5}$ M), were separately added to the media. After incubation in 5% $CO_2$ at 37 °C for 24 h, cell viability was determined by the standard3-[4,5-dimethylthiazol-2-yl]-2,5-diphenyltetrazolium bromide (MTT) assay. As a control experiment, the other group set of cells was exposed to UV irradiation (2.4 μW/$cm^2$) for 5 min after being incubated with MS, MS-FSP, and MS-FSP-CPT for 2 h, and the cell viability was determined after 24 h. The EA.hy926 and HeLa cells viability of free CPT was also carried out for comparison.

**Endocytosis of FD-Loaded MS-FSP by Cancer Cells.** Two samples group of EA.hy926 cells and HeLa cells were seeded on glass-bottom culture dishes ($2 \times 10^4$) and cultured in 5% $CO_2$ at 37 °C for 12 h. Subsequently, FD-loaded MS-FSP, which was dispersed in PBS solution (50 μg/mL), was added into the dishes. After incubation in 5% $CO_2$ at 37 °C for 2 h, one sample group was exposed to UV light (2.4 μW/$cm^2$) for 5 min. Then, the two samples group were incubated for about 12 h, followed by washing cells with PBS solution. Finally, the cells were viewed using confocal microscopy. All images were taken with 488 nm excitation.

**Water Adhesion Detection.** The adhesion force was assessed by microelectromechanical balance system (Kruss) equipped with

a home-built platinum semispherical cap to hold Milli-Q water (10 $\mu$L). The platinum holding water autoapproached the silicon slide sample placed on microelectromechanical balance system platform. As soon as the water touched the surface, the platinum lifted up, and the adhesion force would be monitored. The process was also recorded by CCD as a video.

*Conflict of Interest:* The authors declare no competing financial interest.

*Acknowledgment.* This work is continuously supported by the National Natural Science Foundation of China (Grant Nos. 51173190, 21003132, 21171019, 21073203, 21074139, 51373023, and 21121001), and the 973 Program (2013CB933004, 2011CB932303 and 2011CB808400).

*Supporting Information Available:* The characterization of mesoporous silica nanomaterials, process of preparation of MS-FSP, characterization of MS-FSP by solid-state $^{13}C$ NMR spectroscopy, absorption and emission spectra of fluorescein disodium in water, UV−vis spectra of MS-FSP and MS-FSP-FD in water, XPS characterization of MS-FSP, Table S1, the release process of MS-FSP with different ratio of spiropyran to PFDTES, the FD release of MS-FSP in PBS solution, cell viability of free CPT to EA.hy926 and HeLa cells, and the endocytosis of MS-FSP-FD by HeLa cells. This material is available free of charge *via* the Internet at http://pubs.acs.org.

## REFERENCES AND NOTES

1. Feng, L.; Li, S. H.; Li, Y. S.; Li, H. J.; Zhang, L. J.; Zhai, J.; Song, Y. L.; Liu, B. Q.; Jiang, L.; Zhu, D. B. Super-Hydrophobic Surfaces: From Natural to Artificial. *Adv. Mater.* **2002**, *14*, 1857–1860.
2. Gao, X. F.; Jiang, L. Water-Repellent Legs of Water Striders. *Nature* **2004**, *432*, 36.
3. Parker, A. R.; Lawrence, C. R. Water Capture by a Desert Beetle. *Nature* **2001**, *414*, 33.
4. Zhai, L.; Berg, M. C.; Cebeci, F. C.; Kim, Y.; Milwid, J. M.; Rubner, M. F.; Cohen, R. E. Patterned Superhydrophobic Surfaces: Toward a Synthetic Mimic of the Namib Desert Beetle. *Nano Lett.* **2006**, *6*, 1213–1217.
5. Yao, X.; Song, Y. L.; Jiang, L. Applications of Bio-Inspired Special Wettable Surfaces. *Adv. Mater.* **2011**, *23*, 719–734.
6. Tomsic, B.; Simoncic, B.; Orel, B.; Cerne, L.; Tavcer, P. F.; Zorko, M.; Jerman, I.; Vilcnik, A.; Kovac, J. Sol-Gel Coating of Cellulose Fibres with Antimicrobial and Repellent Properties. *J. Sol−Gel Sci. Technol.* **2008**, *47*, 44–57.
7. Hoefnagels, H. F.; Wu, D.; de With, G.; Ming, W. Biomimetic Superhydrophobic and Highly Oleophobic Cotton Textiles. *Langmuir* **2007**, *23*, 13158–13163.
8. Chaudhury, M. K.; Whitesides, G. M. How To Make Water Run Uphill. *Science* **1992**, *256*, 1539–1541.
9. Ichimura, K.; Oh, S. K.; Nakagawa, M. Light-Driven Motion of Liquids on a Photoresponsive Surface. *Science* **2000**, *288*, 1624–1626.
10. Wang, Z.; Ci, L.; Chen, L.; Nayak, S.; Ajayan, P. M.; Koratkar, N. Polarity-Dependent Electrochemically Controlled Transport of Water through Carbon Nanotube Membranes. *Nano Lett.* **2007**, *7*, 697–702.
11. Feng, L.; Zhang, Z. Y.; Mai, Z. H.; Ma, Y. M.; Liu, B. Q.; Jiang, L.; Zhu, D. B. A Super-Hydrophobic and Super-Oleophilic Coating Mesh Film for the Separation of Oil and Water. *Angew. Chem., Int. Ed.* **2004**, *43*, 2012–2014.
12. Xue, Z.; Wang, S.; Lin, L.; Chen, L.; Liu, M.; Feng, L.; Jiang, L. A Novel Superhydrophilic and Underwater Superoleophobic Hydrogel-Coated Mesh for Oil/Water Separation. *Adv. Mater.* **2011**, *23*, 4270–4273.
13. Jensen, M. O.; Borhani, D. W.; Lindorff-Larsen, K.; Maragakis, P.; Jogini, V.; Eastwood, M. P.; Dror, R. O.; Shaw, D. E. Principles of Conduction and Hydrophobic Gating in $K^+$ Channels. *Proc. Natl. Acad. Sci. U. S. A.* **2010**, *107*, 5833–5838.
14. Anishkin, A.; Sukharev, S. Water Dynamics and Dewetting Transitions in the Small Mechanosensitive Channel MscS. *Biophys. J.* **2004**, *86*, 2883–2895.
15. Powell, M. R.; Cleary, L.; Davenport, M.; Shea, K. J.; Siwy, Z. S. Electric-Field-Induced Wetting and Dewetting in Single Hydrophobic Nanopores. *Nat. Nanotechnol.* **2011**, *6*, 798–802.
16. Smirnov, S. N.; Vlassiouk, I. V.; Lavrik, N. V. Voltage-Gated Hydrophobic Nanopores. *ACS Nano* **2011**, *5*, 7453–7461.
17. Trewyn, B. G.; Giri, S.; Slowing, I. I.; Lin, V. S. Y. Mesoporous Silica Nanoparticle Based Controlled Release, Drug Delivery, and Biosensor Systems. *Chem. Commun.* **2007**, 3236–3245.
18. Liong, M.; Lu, J.; Kovochich, M.; Xia, T.; Ruehm, S. G.; Nel, A. E.; Tamanoi, F.; Zink, J. I. Multifunctional Inorganic Nanoparticles for Imaging, Targeting, and Drug Delivery. *ACS Nano* **2008**, *2*, 889–896.
19. Lai, C. Y.; Trewyn, B. G.; Jeftinija, D. M.; Jeftinija, K.; Xu, S.; Jeftinija, S.; Lin, V. S. Y. A Mesoporous Silica Nanosphere-Based Carrier System with Chemically Removable CdS Nanoparticle Caps for Stimuli-Responsive Controlled Release of Neurotransmitters and Drug Molecules. *J. Am. Chem. Soc.* **2003**, *125*, 4451–4459.
20. Chen, C.; Geng, J.; Pu, F.; Yang, X. J.; Ren, J. S.; Qu, X. G. Polyvalent Nucleic Acid/Mesoporous Silica Nanoparticle Conjugates: Dual Stimuli-Responsive Vehicles for Intracellular Drug Delivery. *Angew. Chem., Int. Ed.* **2011**, *50*, 882–886.
21. Lee, J. E.; Lee, D. J.; Lee, N.; Kim, B. H.; Choi, S. H.; Hyeon, T. Multifunctional Mesoporous Silica Nanocomposite Nanoparticles for pH Controlled Drug Release and Dual Modal Imaging. *J. Mater. Chem.* **2011**, *21*, 16869–16872.
22. Chen, L. F.; Di, J. C.; Cao, C. Y.; Zhao, Y.; Ma, Y.; Luo, J.; Wen, Y. Q.; Song, W. G.; Song, Y. L.; Jiang, L. A pH-Driven DNA Nanoswitch for Responsive Controlled Release. *Chem. Commun.* **2011**, *47*, 2850–2852.
23. Liu, R.; Zhang, Y.; Zhao, X.; Agarwal, A.; Mueller, L. J.; Feng, P. Y. pH-Responsive Nanogated Ensemble Based on Gold-Capped Mesoporous Silica through an Acid-Labile Acetal Linker. *J. Am. Chem. Soc.* **2010**, *132*, 1500–1501.
24. Wang, C.; Li, Z.; Cao, D.; Zhao, Y.-L.; Gaines, J. W.; Bozdemir, O. A.; Ambrogio, M. W.; Frasconi, M.; Botros, Y. Y.; Zink, J. I.; *et al.* Stimulated Release of Size-Selected Cargos in Succession from Mesoporous Silica Nanoparticles. *Angew. Chem., Int. Ed.* **2012**, *51*, 5460–5465.
25. Yang, P.; Gai, S.; Lin, J. Functionalized Mesoporous Silica Materials for Controlled Drug Delivery. *Chem. Soc. Rev.* **2012**, *41*, 3679–3698.
26. Giri, S.; Trewyn, B. G.; Stellmaker, M. P.; Lin, V. S. Y. Stimuli-Responsive Controlled-Release Delivery System Based on Mesoporous Silica Nanorods Capped with Magnetic Nanoparticles. *Angew. Chem., Int. Ed.* **2005**, *44*, 5038–5044.
27. Hernandez, R.; Tseng, H. R.; Wong, J. W.; Stoddart, J. F.; Zink, J. I. An Operational Supramolecular Nanovalve. *J. Am. Chem. Soc.* **2004**, *126*, 3370–3371.
28. Zhao, Y.-L.; Li, Z.; Kabehie, S.; Botros, Y. Y.; Stoddart, J. F.; Zink, J. I. pH-Operated Nanopistons on the Surfaces of Mesoporous Silica Nanoparticles. *J. Am. Chem. Soc.* **2010**, *132*, 13016–13025.
29. Aznar, E.; Casasus, R.; Garcia-Acosta, B.; Marcos, M. D.; Martinez-Manez, R.; Sancenon, F.; Soto, J.; Amoros, P. Photochemical and Chemical Two-Channel Control of Functional Nanogated Hybrid Architectures. *Adv. Mater.* **2007**, *19*, 2228–2231.
30. Soler-Illia, G. J. A. A.; Azzaroni, O. Multifunctional Hybrids by Combining Ordered Mesoporous Materials and Macromolecular Building Blocks. *Chem. Soc. Rev.* **2011**, *40*, 1107–1150.
31. Angelatos, A. S.; Wang, Y. J.; Caruso, F. Probing the Conformation of Polyeletrolytes in Mesoporous Silica Spheres. *Langmuir* **2008**, *24*, 4224–4230.
32. Staff, R. H.; Gallei, M.; Mazurowski, M.; Rehahn, M.; Berger, R.; Landfester, K.; Crespy, D. Patchy Nanocapsules of Poly(vinylferrocene)-Based Block Copolymers for Redox-Responsive Release. *ACS Nano* **2012**, *6*, 9042–9049.
33. Yang, Q.; Wang, S. C.; Fan, P. W.; Wang, L. F.; Di, Y.; Lin, K. F.; Xiao, F. S. pH-Responsive Carrier System Based on Carboxylic Acid Modified Mesoporous Silica and Polyelectrolyte for Drug Delivery. *Chem. Mater.* **2005**, *17*, 5999–6003.

34. Park, C.; Oh, K.; Lee, S. C.; Kim, C. Controlled Release of Guest Molecules from Mesoporous Silica Particles Based on a pH-Responsive Polypseudorotaxane Motif. *Angew. Chem., Int. Ed.* **2007**, *46*, 1455–1457.
35. Yohe, S. T.; Colson, Y. L.; Grinstaff, M. W. Superhydrophobic Materials for Tunable Drug Release: Using Displacement of Air To Control Delivery Rates. *J. Am. Chem. Soc.* **2012**, *134*, 2016–2019.
36. Klajn, R. Spiropyran-Based Dynamic Materials. *Chem. Soc. Rev.* **2013**, *43*, 148–184.
37. Such, G.; Evans, R. A.; Yee, L. H.; Davis, T. P. Factors Influencing Photochromism of Spiro-Compounds within Polymeric Matrices. *J. Macromol. Sci., Polym. Rev.* **2003**, *43*, 547–579.
38. Ercole, F.; Davis, T. P.; Evans, R. A. Photo-Responsive Systems and Biomaterials: Photochromic Polymers, Light-Triggered Self-Assembly, Surface Modification, Fluorescence Modulation and Beyond. *Polym. Chem.* **2010**, *1*, 37–54.
39. Rosario, R.; Gust, D.; Hayes, M.; Jahnke, F.; Springer, J.; Garcia, A. A. Photon-Modulated Wettability Changes on Spiropyran-Coated Surfaces. *Langmuir* **2002**, *18*, 8062–8069.
40. Dattilo, D.; Armelao, L.; Fois, G.; Mistura, G.; Maggini, M. Wetting Properties of Flat and Porous Silicon Surfaces Coated with a Spiropyran. *Langmuir* **2007**, *23*, 12945–12950.
41. Vlassiouk, I.; Park, C. D.; Vail, S. A.; Gust, D.; Smirnov, S. Control of Nanopore Wetting by a Photochromic Spiropyran: A Light-Controlled Valve and Electrical Switch. *Nano Lett.* **2006**, *6*, 1013–1017.
42. Grun, M.; Lauer, I.; Unger, K. K. The Synthesis of Micrometer- and Submicrometer-Size Spheres of Ordered Mesoporous Oxide MCM-41. *Adv. Mater.* **1997**, *9*, 254–257.
43. Samanta, S.; Locklin, J. Formation of Photochromic Spiropyran Polymer Brushes *via* Surface-Initiated, Ring-Opening Metathesis Polymerization: Reversible Photocontrol of Wetting Behavior and Solvent Dependent Morphology Changes. *Langmuir* **2008**, *24*, 9558–9565.